sustainability

MDPI

Article

Evaluation and Prediction of Carbon Storage in the Qinghai-Tibet Plateau by Coupling the GMMOP and PLUS Models

Li Yuan [1], Jing Xu [1] and Binrui Feng [2,*]

[1] School of Agricultural and Forestry Economics and Management, Lanzhou University of Finance and Economics, Lanzhou 730101, China; wanl@lzufe.edu.cn (L.Y.); xujing@lzufe.edu.cn (J.X.)
[2] School of Economics, Lanzhou University of Finance and Economics, Lanzhou 730101, China
* Correspondence: edubrian@163.com

Abstract: Land-use alterations exert a profound impact on carbon storage within terrestrial ecosystems. Exploring the spatiotemporal dynamics of regional land use and carbon storage is crucial for optimizing national spatial planning and fostering low-carbon development. For this study, we utilized land-use data spanning from 2000 to 2020 for the Tibetan Plateau and assessed the spatial and temporal variations in carbon storage using the Integrated Valuation of Ecosystem Services and Tradeoffs (InVEST) model. We adjusted the carbon density within the provinces in the study area as a prerequisite. Moreover, we integrated the Grey Multi-objective Decision-making (GMMOP) model with the Patch-generating Land-use Simulation (PLUS) model to forecast carbon storage alterations in 2030 across various scenarios. The findings indicated that between 2000 and 2020, the overall carbon storage witnessed a decrease of 18.94×10^8 t. Carbon storage in grassland decreased by 22.10×10^8 t, and carbon storage in unused land, forest land, cultivated land, construction land, and water increased by 1.56×10^8 t, 0.92×10^8 t, 0.66×10^8 t, 158.50×10^4 t and 26.74×10^4 t, respectively. The soil organic carbon pool exhibited the highest average carbon storage of 195.63×10^8 t, whereas the litterfall organic carbon pool contained the lowest average carbon stock of 15.07×10^8 t. In comparison with the levels observed in 2020, the total carbon storage experienced a reduction of 8.66×10^8 t and 5.29×10^8 t under the inherent progression and economic growth scenarios, respectively. Conversely, it rose by 11.87×10^8 t and 16.21×10^8 t under the environmental preservation and holistic progression scenarios, respectively. Under the holistic progression scenario, the belowground biomass organic carbon pool exhibited the highest carbon storage increase of 5.59%. These findings offer valuable insights for the management and enhancement of carbon sinks in the Qinghai-Tibet Plateau.

Keywords: carbon storage; land use; GMMOP-PLUS model; the Qinghai-Tibet Plateau

Citation: Yuan, L.; Xu, J.; Feng, B. Evaluation and Prediction of Carbon Storage in the Qinghai-Tibet Plateau by Coupling the GMMOP and PLUS Models. *Sustainability* **2024**, *16*, 5776. https://doi.org/10.3390/su16135776

Academic Editor: Ali Bahadori-Jahromi

Received: 6 May 2024
Revised: 1 July 2024
Accepted: 4 July 2024
Published: 6 July 2024

1. Introduction

Terrestrial ecosystems, as vital carbon reservoirs in the carbon cycle, play a pivotal role in maintaining the balance of global carbon levels and promoting climate stability [1]. Consequently, they have garnered significant attention from governments and scholars worldwide [2]. Alterations in land use significantly influence regional carbon sources, sinks, and carbon-cycle dynamics by modifying ecosystem structures and functions [3]. Consequently, land-use change constitutes a pivotal factor contributing to fluctuations in carbon stocks within terrestrial ecosystems [4]. A thorough assessment and forecasting of land-use change, coupled with the resulting spatial and temporal fluctuations in carbon stocks, not only facilitate the achievement of dual-carbon objectives but also offer valuable insights for fostering high-quality economic and social development.

Terrestrial ecosystems represent some of the Earth's largest carbon reservoirs, and they accomplish carbon sequestration by capturing atmospheric CO_2 through plant pho-

tosynthesis [5]. This process typically involves four carbon pools: aboveground biomass organic carbon, belowground biomass organic carbon, litterfall organic carbon, and soil organic carbon [6]. In the early analysis of biological carbon stocks in terrestrial ecosystems, biomass conversion factors were predominantly utilized. This method involved establishing a regression relationship between biomass and the carbon stock volume [7,8]. Litterfall organic carbon stock assessment has largely been used for regional sampling statistics [9]. Terrestrial soil organic carbon stocks are generally measured using the soil-type method [10]. The rapid advancement of geographic information technology, coupled with the widespread use of high-resolution remote sensing data in natural resource surveys, has led to the emergence of regional carbon sink assessment methodologies based on land-use/land-cover change (LUCC) [11,12]. This approach has become a crucial research method in the field [13]. Currently, the system dynamics (SD) [14], conversion of land use and its effects at small region extent (CLUE-S) [15], future land-use simulation (FLUS) [16], patch-generating land-use simulation (PLUS) [17], and other models are mostly used to explore the dynamic evolution of land use. The PLUS model stands out for its high simulation accuracy that is primarily attributed to the integration of a multitype stochastic seeding mechanism and a land expansion analysis strategy, which can be employed to determine land expansion and landscape dynamic drivers and to predict land-use patch-level evolution [18,19]. Carbon stock assessment primarily adopts models such as the denitrification decomposition (DNDC) [20], artificial intelligence for ecosystem services (ARIES) [21], social values for ecosystem services (SolVES) [22], and integrated valuation of ecosystem services and tradeoffs (InVEST) models [23]. The InVEST model excels in simulating carbon stocks in terrestrial ecosystems by accounting for spatial and temporal changes in land use/land cover (LULC). Its key strengths lie in its straightforward model inputs and broad applicability, making it the most suitable model currently available for simulating carbon stocks in terrestrial ecosystems. With the advantages of simple model inputs and a wide application range, this model is one of the more mature models for carbon stock assessment [24,25]. The study scale has gradually increased from single cities to urban agglomerations, watersheds or regions, but large-scale study areas often span multiple climatic zones, and the temperature and precipitation levels between different climatic zones usually vary significantly [26], thus affecting the carbon density of biomass organic carbon and soil organic carbon [27]. Nevertheless, most existing studies entailed the use of a single carbon density for carbon stock measurement, ignoring the differences in climatic environments between regions, which may have led to notable errors in the results [28]. In addition, existing carbon stock assessment studies have gradually shifted from deducing the history and current situation to predicting future development. Existing studies have primarily concentrated on forecasting spatial and temporal variations in carbon stocks using models such as SD [14], CLUE-S [29], cellular automata (CA)-Markov, and others [30]. However, they frequently fail to consider the potential impact of land-use changes; moreover, there are problems such as the difficulty in determining parameters and high randomness [31]. However, the grey multi-objective decision-making (GMMOP) model integrates gray prediction theory and multi-objective linear programming, which can not only solve the uncertainties in objective functions and constraints but also address problems in the prediction of quantity structures [32,33]. At present, few studies have considered coupling the GMMOP, PLUS, and InVEST models to achieve carbon stock prediction, and the validity of these models should be further assessed and explored. The GMMOP model integrates multi-objective linear programming with gray prediction theory, which not only addresses various uncertainties in objective functions and constraints but also resolves multi-objective conflicts in quantitative structure prediction. This model has the advantage of reflecting the evolution characteristics of dynamic processes. In terms of spatial distribution prediction, the PLUS model incorporates multi-type random-seed mechanisms and land expansion analysis strategies. It can uncover the driving factors of land expansion and landscape dynamics and predict the patch-level evolution of land use with high simulation accuracy. As it is a newly developed predictive model, few studies

have combined GMMOP with PLUS for the assessment and prediction of carbon stocks. The effectiveness of this model coupling requires further validation and exploration.

Carbon stocks play a crucial role in the global carbon cycle, and studying them is vital for addressing climate change. By predicting changes in carbon sinks and sources, effective emission reduction strategies and carbon management policies can be developed to reduce greenhouse gas emissions and mitigate global warming. The Qinghai-Tibet Plateau, with an average altitude of over 4000 m, is known as the "Third Pole of the Earth" and the "Water Tower of Asia" [34]. Its high altitude and low temperatures make it the most significant permafrost concentration area in the low-latitude regions [35]. The carbon stock in the Qinghai-Tibet Plateau is unique. As an area sensitive to global climate change, its distinctive geographic and climatic conditions make carbon stock research in this region particularly important [36]. Therefore, scientifically assessing the historical evolution of carbon stocks in the Qinghai-Tibet Plateau and predicting their dynamic changes under different scenarios are crucial. This not only directly impacts the achievement of China's "dual carbon" goals but also concerns regional ecological security and high-quality socioeconomic development. Although significant progress has been made in global carbon stock and carbon cycle research, the Qinghai-Tibet Plateau's position in these studies and the existing research gaps remain evident. Further in-depth research on the dynamic changes of carbon stocks in the Qinghai-Tibet Plateau is of great scientific significance for understanding global climate change and its ecological and environmental impacts. Hence, for this study, land-use data spanning from 2000 to 2020 were collected for the Tibetan Plateau. Building upon the correction of carbon density within each province in the study area, the InVEST model was employed to evaluate the spatial and temporal fluctuations in carbon stocks across the Tibetan Plateau. Furthermore, the study integrated the GMMOP-PLUS model to forecast the trajectory of carbon stock changes under various development scenarios. This endeavor aimed to furnish a foundational reference for safeguarding and augmenting carbon sink capabilities within the Tibetan Plateau region.

2. Study Area and Data Sources

2.1. Study Area

The Tibetan Plateau (26°00′ N~39°47′ N, 73°18′ E~104°47′ E), situated in South–Central Asia, occupies the third terrace in Western China. It stretches from the Qilian Mountains and Kunlun Mountains in the north to the Himalayas in the south, and from the Pamir Plateau in the west to the Hengduan Mountain Range and Loess Plateau in the east. This vast region encompasses six provinces and autonomous regions, including the Tibet Autonomous Region (TAR), Qinghai Province, Sichuan Province, Yunnan Province, Gansu Province, and Xinjiang Uygur Autonomous Region. The Qinghai Province, Sichuan Province, Yunnan Province, Gansu Province, and Xinjiang Uygur Autonomous Region collectively cover an approximate area of 2.582 million km^2 [37,38]. The average elevation exceeds 4000 m and spans three climatic zones, with obvious regional differences in geographic characteristics [39]. The ecosystem types are complex and diverse, including forests, grasslands, farmlands, wetlands, shrublands, deserts, and lakes. Among these, grassland ecosystems occupy roughly 60% of the total area. The total population is approximately 13,134,000 people, accounting for only 0.9% of the total population of China, with an overall urbanization rate of approximately 47.6% [40], and the gap between the level of economic growth here and that of developed regions in the east is notable (Figure 1).

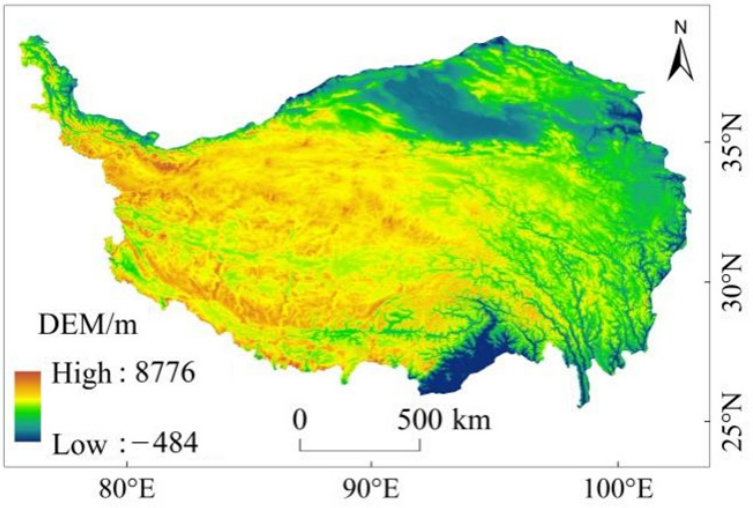

Figure 1. Geographical location of the study region.

2.2. Data Sources

The data utilized in this study were sourced from both domestic and international public databases. Among them, the land-use data originated from the GlobeLand30 global land-cover data (http://www.globallandcover.com/) (accessed on 23 May 2023), which was resampled at 300 m resolution and reclassified as cultivated land, forest land, grassland, watershed, construction land, and unused land; the elevation model was from the Geospatial Data Cloud (https://www.gscloud.cn/#page1/3) (accessed on 23 May 2023); the slope and slope direction factors were extracted using the 3D analysis module in ArcGIS; meteorological data were obtained from the National Earth System Science Data Center (http://www.geodata.cn/) (accessed on 23 May 2023); the Normalized Vegetation Index (NDVI) was obtained from the National Science and Technology Resource Sharing Service Platform (www.cas.cn) (accessed on 23 May 2023); the distance to the road was obtained from the OpenStreetMap website (www.openhistoricalmap.org) (accessed on 23 May 2023); the distance to the river was obtained from the National Geographic Information Resource Catalog Service System (www.webmap.cn) (accessed on 23 May 2023); and the population density and GDP data were obtained from the Resource and Environment Science and Data Center of the Chinese Academy of Sciences (www.resdc.cn) (accessed on 23 May 2023).

3. Research Methodology

The research framework is illustrated in Figure 2. Initially, the PLUS method is employed to extract data on land expansion across the Tibetan Plateau from 2000 to 2020. The initiation of the LEAS module marks the beginning of endeavors to quantify the influence of driving factors on specific land-use types. Following this, the CARS module is employed to predict the future development potential of each land-use type. Subsequently, the land-use and land-cover change (LUCC) patterns observed in the Tibetan Plateau in 2000 are utilized as the foundation for projecting the LUCC in 2020. Comparative analyses are performed to validate the model's accuracy by comparing the predicted and actual land-use distributions in 2020. Additionally, the GMMOP model is utilized, integrating future scenario settings and conversion conditions to calculate the number of LUCC patches in 2030. Subsequently, the InVEST model is utilized to assess the carbon storage distribution across various scenarios spanning the years 2000, 2010, 2020, and 2030. Finally, spatial autocorrelation analysis is conducted to perform cluster analyses on future scenario carbon storage projections.

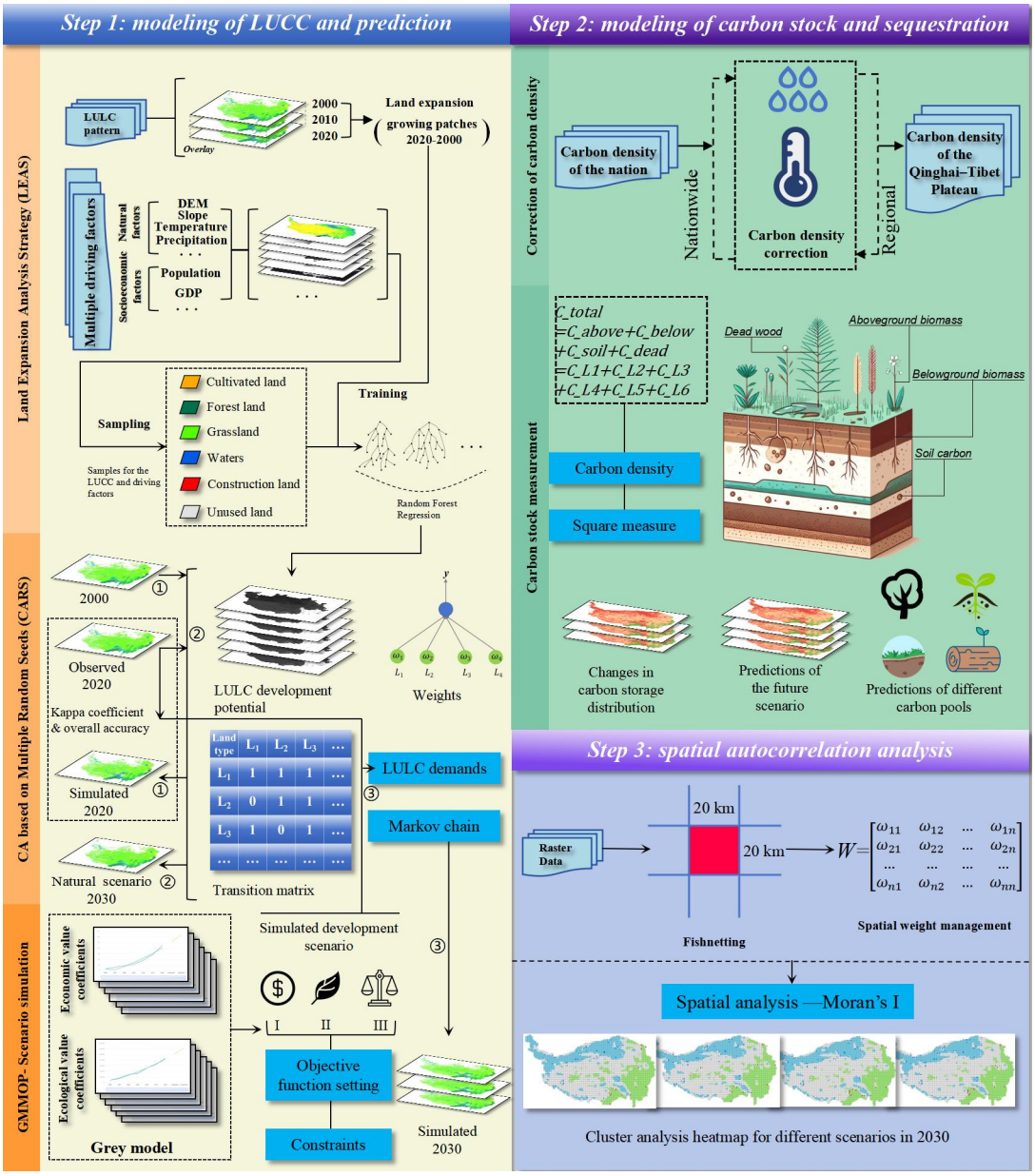

Figure 2. Methodological framework used in this study.

3.1. Carbon Density Correction and Carbon Stock Measurement

3.1.1. Carbon Density Correction

In accordance with the findings of Alam et al. (2013) [41], adjustments were made to the carbon density model, incorporating regional average annual precipitation and average annual temperature data. This adjustment facilitated the derivation of the average carbon density within the study area.

$$C_{SP} = 3.3968 \times P + 3996.1 \quad (1)$$

$$C_{BP} = 6.798e^{\,0.0054P} \quad (2)$$

$$C_{BT} = 28 \times T + 398 \quad (3)$$

In the equation, C_{SP} represents the soil carbon density determined by the average annual precipitation, while C_{BP} and C_{BT} denote the biomass carbon densities derived from the

average annual precipitation and average annual temperature, respectively. Additionally, P signifies the average annual precipitation, and T denotes the average annual temperature.

$$K_{BP} = \frac{C'_{BP}}{C''_{BP}} \quad (4)$$

$$K_{BT} = \frac{C'_{BT}}{C''_{BT}} \quad (5)$$

$$K_B = K_{BP} \times K_{BT} \quad (6)$$

$$K_S = \frac{C'_{SP}}{C''_{SP}} \quad (7)$$

In the equation, K_{BP}, K_{BT}, K_B, and K_S represent correction factors for the biomass carbon density based on precipitation, correction factors for the biomass carbon density based on temperature, correction factors for the biomass carbon density, and correction factors for soil carbon density, respectively; C'_{BP} represents the biomass carbon density of the Tibetan Plateau based on the average annual precipitation, while C''_{BP} denotes the biomass carbon density of the entire country under the same parameter; C'_{BT} represents the biomass carbon density of the Tibetan Plateau based on the annual mean temperature, while C''_{BT} denotes the biomass carbon density of the entire country under the same parameter; C'_{SP} represents the soil carbon density of the Tibetan Plateau based on annual mean temperature, while C''_{SP} denotes the soil carbon density of the entire country under the same parameter. The carbon density was calculated based on Yang et al. (2021) [42], referencing the "carbon density of land-use/land-cover in China". The specific details are as follows (Table 1):

Table 1. Average carbon density of various land-use/cover types in China (t·km^{-2}).

Land Type	C_a	C_b	C_s	C_d
Cultivated land	17.0	80.7	108.4	9.8
Forest land	42.4	115.9	158.8	14.1
Grassland	35.3	86.5	99.9	7.3
Water	0.3	0	0	0
Construction land	2.5	27.5	0	0
Unused land	1.3	0	21.6	0

Note: C_a, C_b, C_s, and C_d represent the aboveground biomass, belowground biomass, soil, and litterfall organic matter carbon stocks, respectively.

Based on the average carbon density of various land-use/cover types in China, the carbon density for each province is adjusted using Formulas (1)–(7). This results in the land carbon density for the provinces of the Qinghai-Tibet Plateau, as shown in Table 2.

Table 2. Carbon density of land-use/land-cover of six provinces of the Qinghai-Tibet Plateau (t·km^{-2}).

Land Type	Gansu				Qinghai				Sichuan			
	C_a	C_b	C_s	C_d	C_a	C_b	C_s	C_d	C_a	C_b	C_s	C_d
Cultivated land	229.78	1090.76	8796.74	982.36	226.67	1076.03	9230.25	982.36	7353.66	34,908.24	12,508.90	982.36
Forest land	573.09	1566.53	12,886.74	1411.17	565.35	1545.38	13,521.80	1411.17	18,340.88	50,134.63	18,324.85	1411.17
Grassland	477.12	1169.16	8106.96	727.59	470.68	1153.37	8506.48	727.59	15,269.65	37,417.13	11,528.04	727.59
Water	4.05	0.00	0.00	0.00	4.00	0.00	0.00	0.00	129.77	0.00	0.00	0.00
Construction land	33.79	371.70	0.00	0.00	33.33	366.68	0.00	0.00	1081.42	11,895.62	0.00	0.00
Unused land	17.57	0.00	1752.86	0.00	17.33	0.00	1839.24	0.00	562.34	0.00	2492.55	0.00
Land Type	**Xinjiang**				**Tibet**				**Yunnan**			
	C_a	C_b	C_s	C_d	C_a	C_b	C_s	C_d	C_a	C_b	C_s	C_d
Cultivated land	134.91	640.43	8211.27	982.36	439.28	2085.29	9886.22	982.36	14,041.24	66,654.60	13,039.20	982.36
Forest land	336.49	919.78	12,029.06	1411.17	1095.62	2994.85	14,482.76	1411.17	35,020.51	95,728.22	19,101.71	1411.17
Grassland	280.14	686.46	7567.40	727.59	912.15	2235.16	9111.01	727.59	29,156.22	71,445.14	12,016.75	727.59
Water	2.38	0.00	0.00	0.00	7.75	0.00	0.00	0.00	247.79	0.00	0.00	0.00
Construction land	19.84	218.24	0.00	0.00	64.60	710.60	0.00	0.00	2064.89	22,713.77	0.00	0.00
Unused land	10.32	0.00	1636.19	0.00	33.59	0.00	1969.95	0.00	1073.74	0.00	2598.22	0.00

3.1.2. Carbon Stock Measurement

The carbon stocks of the four types of carbon pools, namely aboveground biomass, belowground biomass, soil, and litterfall organic matter, were estimated based on LULC as follows [43]:

$$C_j = C_{ja} + C_{jb} + C_{js} + C_{jd} \quad (8)$$

$$C_T = \sum_{j=1}^{n} S_j \times C_j \quad (9)$$

where C_{ja}, C_{jb}, C_{js}, and C_{jd} are the carbon densities of the aboveground biomass, belowground biomass, soil, and litterfall organic matter carbon pools of land-use type j; C_j and S_j are the total carbon density and area, respectively, of land-use type j; C_T is the total carbon stock; and n is the number of land-use types.

3.2. GMMOP-Based Development Scenario Simulation

The GMMOP model combines gray modeling (GM) with multi-objective planning (MOP), which aims to evaluate the relative importance among objectives through gray correlation, and uses the MOP model to perform assessments and decision-making under the premise of satisfying multiple objectives.

3.2.1. Land-Use Value Coefficient

The values created by agriculture, forestry, animal husbandry, fishery, and secondary and tertiary industries per unit area from 2010 to 2020 were used as the economic value coefficients for cultivated land, forest land, grassland, watershed, and construction land, respectively [44], and the value of unused land was set to 0 [45]. The ecosystem service value per unit area of each category was utilized as the ecological value coefficient [18,46]. Based on the value coefficients from 2010 to 2020, the economic value coefficients and ecological value coefficients of each category were forecasted for 2030 using the GM (1.1) model, as outlined in Table 3.

Table 3. Ecological and economic value coefficients of the different types of land use in the Qinghai-Tibet Plateau in 2030.

Value Coefficient (10^4 Yuan·km^{-2})	Cultivated Land	Forest land	Grassland	Water	Construction Land	Unused Land
Ecological value	77.37	488.78	327.38	2085.50	0	15.59
Economic value	291.83	21.31	35.69	12.55	15,024.70	0

3.2.2. Scenario Setting and Objective Function Construction

In this study, the four scenarios of inherent progression, economic growth, environmental preservation, and holistic progression were established with the following constraints and objective functions under each scenario:

The inherent progression scenario is not subject to policy constraints and is obtained via CA-Markov prediction.

The economic growth scenario aims to guarantee the maximum economic value in the study area:

$$V_{ed}(X) = \text{Max} \sum_{j=1}^{6} E_j \times S_j \quad (10)$$

The ecological conservation scenario aims to safeguard the maximum ecological value in the study area:

$$V_{ep}(X) = \text{Max} \sum_{j=1}^{6} P_j \times S_j \quad (11)$$

The integrated development scenario aims to promote synergistic ecological and economic growth [47]:

$$V_{cd}(X) = Max\{V_{ed}(X), V_{ep}(X)\} \quad (12)$$

where V_{ed} (X), V_{ep} (X), and V_{cd} (X) are the total values under the economic growth, environmental preservation, and integrated development scenarios, respectively (in descending order); E_j and P_j are the economic and ecological value coefficients, respectively; j is the land-use type; 1–6 denote cultivated land, forest land, grassland, watershed, construction land, and unused land; and Sj is the area of each land-use type.

Various constraints for land-use prediction were defined for each development scenario [48], as summarized in Table 4.

Table 4. Constraints in land-use prediction.

Constraint Type	Constraint Factor	Constraint Expression
Total	Land area	$\sum_{j=1}^{6} S_j = 258.13$
Economic value	Land area	$\sum_{j=1}^{6} E_j \times S_j \geq \sum_{j=1}^{6} E_j \times N_j$
Economic value	Land area	$\sum_{j=1}^{6} E_j \times S_j \geq 8751.56$
Ecological value	Land area	$\sum_{j=1}^{6} P_j \times S_j \geq \sum_{j=1}^{6} P_j \times N_j$
Ecological value	Land area	$\sum_{j=1}^{6} P_j \times S_j \geq 82.662.22$
Total carbon storage	Land area	$\sum_{j=1}^{6} C_j \times S_j \geq \sum_{j=1}^{6} C_j \times N_j$
Cultivated land	Cultivated land area	$S_1 \geq 2.75$
Unused land	Unused land area	$S_6 \leq 69.69$
Land diversity	Area of forest land, grassland and water bodies	$S_2 + S_3 + S_4 \geq N_2 + N_3 + N_4$
Model accuracy	Land area	$1.1 \times N_j \geq S_j \geq 0.9 \times N_j$

Note: N_j denotes the area of each site type under the inherent progression scenario, and the remaining parameters have the same meaning as above.

3.3. Land-Use Prediction Based on the PLUS Model

3.3.1. Land-Use Drivers

Land-use change is a consequence of a confluence of natural, social, and economic factors. While physical and chemical factors play a role, social and economic factors are pivotal in determining land-use change [49,50]. According to land-use change driver-related research [51,52], seven natural factors (elevation, slope, slope direction, average annual temperature, average annual precipitation, NDVI, and distance from rivers) and four socioeconomic factors (population density, GDP spatial distribution grid, distance from railroads, and distance from highways) were selected as the driving factors in this study.

3.3.2. Conversion Cost Matrix

The land conversion cost matrix delineates the conversion rules governing transitions between various land-use types [53], i.e., low-grade land can be converted into high-grade land, and vice versa. In the conversion cost matrix, a value of 1 signifies that the land-use type can undergo conversion, whereas a value of 0 indicates the opposite, i.e., no conversion is feasible (Table 5).

Table 5. Land-use transfer cost matrix under the different development scenarios.

	Inherent Progression						**Economic Growth**						**Environmental Preservation**						**Holistic Progression**					
	a	b	c	d	e	f	a	b	c	d	e	f	a	b	c	d	e	f	a	b	c	d	e	f
a	1	1	1	1	1	1	1	0	0	0	1	0	1	1	1	1	0	0	1	1	1	0	0	0
b	1	1	1	1	1	1	1	1	1	0	1	0	0	1	0	1	0	0	0	1	0	0	0	0
c	1	1	1	1	1	1	1	0	1	0	1	0	0	1	1	1	0	0	0	1	1	0	0	0
d	1	1	1	1	1	1	1	1	1	1	1	0	0	0	0	1	0	0	1	1	1	1	1	1
e	1	1	1	1	1	1	0	0	0	0	1	0	1	1	1	1	1	1	1	1	1	0	1	1
f	1	1	1	1	1	1	1	1	1	1	1	1	1	1	1	1	0	1	1	1	1	0	0	1

Note: a, b, c, d, e, and f denote cultivated land, forest land, grassland, watersheds, construction land, and unused land, respectively.

3.4. Model Accuracy Verification

Predictions for land use in 2020 were generated based on the land-use patterns observed in 2010. Subsequently, the accuracy of these prediction results was evaluated. The results indicated a kappa coefficient of 0.80 and an overall accuracy of 88.12%, meeting the research requirements.

3.5. Local Spatial Autocorrelation Analysis

This study divided the area into 9347 grids of 20 km × 20 km each, and used the univariate local Moran's I index to measure the spatial clustering characteristics of carbon storage within these grids.

4. Results and Analysis

4.1. Land-Use Changes in the Tibetan Plateau from 2000 to 2020

Grassland exhibited the highest area proportion in the study area (Figure 3), followed by unused land, forest land, watersheds, cultivated land, and construction land. From 2000 to 2020, the grassland area decreased the most, by 127,100 km^2, while the unused land area increased the most, by 85,700 km^2. The highest change rate in land use was observed for construction land (240.00%), followed by water (26.76%), cultivated land (17.02%), unused land (14.02%), grassland (7.90%), and forest land (0.64%) (Table 6).

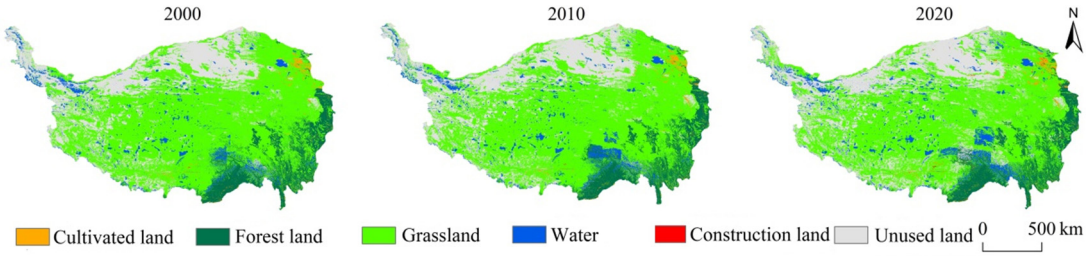

Figure 3. Changes in land use in the Qinghai-Tibet Plateau from 2000 to 2020.

Table 6. Area and proportion of the different land-use types in the Qinghai-Tibet Plateau from 2000 to 2020.

Land Type	**2000**		**2010**		**2020**	
	Area/10^4 km^2	**Proportion/%**	**Area/10^4 km^2**	**Proportion/%**	**Area/10^4 km^2**	**Proportion/%**
Cultivated land	2.35	0.90	2.34	0.89	2.75	1.05
Forest land	24.88	9.50	24.50	9.36	25.04	9.56
Grassland	160.92	61.46	157.56	60.17	148.21	56.60
Water	12.48	4.77	13.86	5.29	15.82	6.04
Construction land	0.1	0.04	0.12	0.05	0.34	0.13
Unused land	61.12	23.34	63.47	24.24	69.69	26.61

4.2. Changes in Carbon Stocks in the Tibetan Plateau from 2000 to 2020

The spatial distribution of carbon stocks in the study area exhibited a decreasing trend from southeast to northwest. High-value areas were predominantly located in southern Tibet and western Sichuan, while medium-value areas were mainly observed in central Tibet and eastern and southern Qinghai. Low-value areas were mostly concentrated in northern Tibet and southern Xinjiang (Figure 4). In 2000, 2010, and 2020, the carbon stocks reached 44,249, 43,480, and 42,355 Mt, respectively, showing a decreasing trend.

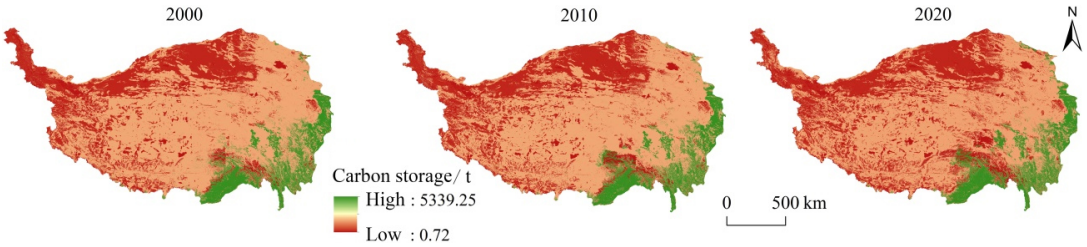

Figure 4. Changes in the carbon storage distribution in the Qinghai-Tibet Plateau from 2000 to 2020.

Concerning land-use types, grassland emerged as the primary contributor to the carbon sink in the Tibetan Plateau, constituting approximately 62.38% of the total carbon stock. This was followed by forest land, unused land, and cultivated land, which accounted for 33.95%, 2.73%, and 0.94%, respectively. From 2000 to 2020, the carbon stock in grassland witnessed a decline of 2210 Mt, while the carbon stocks in forest land, unused land, cultivated land, construction land, and watersheds increased by 92, 156, 66, 15,850, and 2674 Mt, respectively (Table 7).

Table 7. Carbon storage of different land use types in the Qinghai-Tibet Plateau from 2000 to 2020.

Land Type	2000		2010		2020	
	Carbon Storage/10^8 t	Proportion/%	Carbon Storage/10^8 t	Proportion/%	Carbon Storage/10^8 t	Proportion/%
Cultivated land	3.86	0.87	3.85	0.89	4.53	1.07
Forest land	147.62	33.36	145.35	33.43	148.54	35.07
Grassland	279.86	63.25	274.02	63.02	257.76	60.86
Water	0.01	0.00	0.01	0.00	0.01	0.00
Construction land	0.01	0.00	0.01	0.00	0.02	0.01
Unused land	11.14	2.52	11.56	2.66	12.70	3.00

Regarding the types of carbon pools, the Tibetan Plateau's soil organic carbon pool showcased the highest carbon stock, followed by the belowground biomass organic carbon pool. Conversely, the litterfall organic carbon pool encompassed the lowest carbon stock. Between 2000 and 2020, the carbon stocks of the four types of carbon pools all declined (Table 8), with the litterfall organic carbon pool showing the greatest decrease of 5.63%, and the soil, aboveground biomass, and belowground biomass organic carbon pools declining by 4.68%, 4.03%, and 3.76%, respectively.

Table 8. Carbon storage of the different carbon sinks in the Qinghai-Tibet Plateau from 2000 to 2020.

Carbon Pool Type	2000 (10^8 t)	2010 (10^8 t)	2020 (10^8 t)
Aboveground biomass organic carbon	63.52	62.36	60.96
Belowground biomass organic carbon	163.68	160.70	157.52
Litterfall organic carbon	15.46	15.16	14.59
Soil organic carbon	199.83	196.57	190.48

4.3. Land-Use Change in the Tibetan Plateau under the Different Development Scenarios

Compared with 2020, under the inherent progression scenario, only the grassland area experienced a decrease, of 750,000 km^2, while the areas of all other land types increased (Table 8). New unused land was mainly located in Tibet in Yushu, Qinghai, Nagchu, and Shigatse, and water areas also largely occurred in Tibet in Linzhi, Nagchu, and Chamdo (Figure 5). Under the economic growth scenario, the areas of grassland, cultivated land, and construction land increased by 36,100 km^2, 0.67 million km^2, and 0.24 million km^2, respectively. Conversely, the areas of forest land and unused land decreased by 20,600 km^2 and 24,600 km^2, respectively, with newly added grassland mainly occurring in Ganzi and Aba of Sichuan Province and Liangshan Mountain. Under the environmental preservation scenario, the forest land and water areas rapidly increased, by 30,300 and 25,600 km^2, respectively, with new forest land largely located in Linzhi (Tibet), Ganzi (Sichuan), and Aba (Sichuan), and water mostly occurring in Nagchu and Chamdo (Tibet) and Yushu (Qinghai). In contrast, the areas of grassland and unused land experienced decreases of 33,200 km^2 and 24,600 km^2, respectively. Under the integrated development scenario, the grassland area decreased by 14,100 km^2, while the construction land area increased by 0.17 million km^2 (Table 9). The newly developed construction land was predominantly situated in Lhasa (Tibet), as well as in Xining and Haidong (Qinghai).

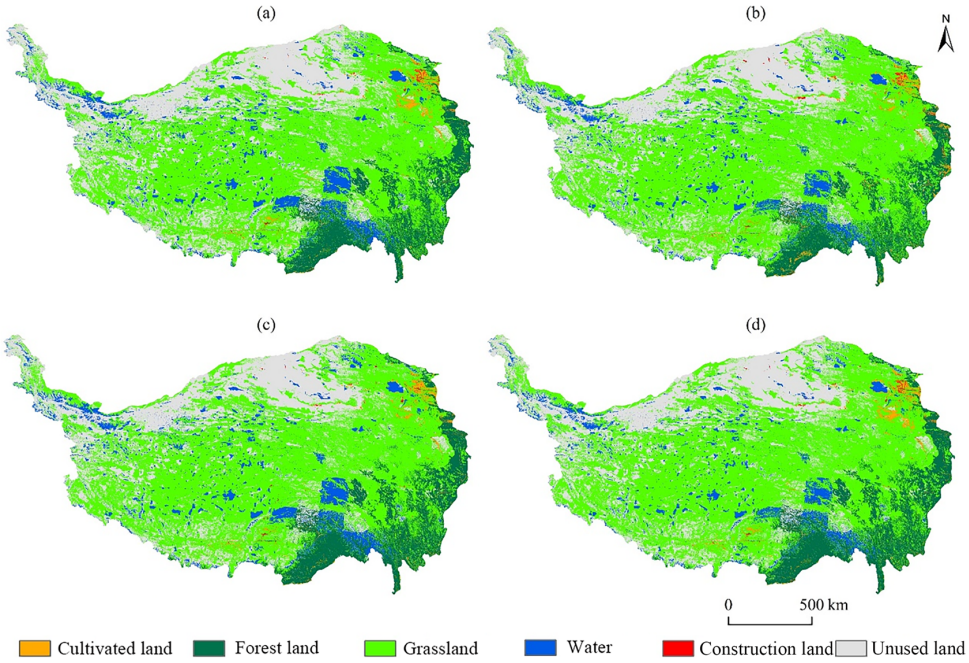

Figure 5. Land-use distribution in the Qinghai-Tibet Plateau under the different development scenarios in 2030. (**a**) Inherent progression scenario; (**b**) Economic growth scenario; (**c**) Environmental preservation scenario; (**d**) Holistic progression scenario.

Table 9. Changes in the land-use area in the Qinghai-Tibet Plateau under the different development scenarios in 2030.

Land Type	Inherent Progression (10^4 km^2)	Economic Growth (10^4 km^2)	Environmental Preservation (10^4 km^2)	Holistic Progression (10^4 km^2)
Cultivated land	0.36	0.67	0.05	0.67
Forest land	0.48	−2.06	3.03	3.03
Grassland	−7.50	3.61	−3.32	−1.41
Water	1.46	0.00	2.56	0.00
Construction land	0.19	0.24	0.14	0.17
Unused land	5.01	−2.46	−2.46	−2.46

4.4. Carbon Stock Changes in the Tibetan Plateau under the Different Development Scenarios

In 2030, the carbon stock was highest under the holistic progression scenario, reaching 43,976 Mt, and lowest was under the inherent progression scenario, at 41,489 Mt (Table 9). In contrast with the carbon stocks observed in 2020, the inherent progression and economic growth scenarios experienced declines of 2.05% and 1.25%, respectively. Conversely, the environmental preservation and holistic progression scenarios saw increases of 2.80% and 3.83%, respectively. Under the inherent progression scenario, the newly increased carbon stock was mainly distributed in Linzhi and Chamdo of Tibet and Ganzi of Sichuan Province, and the reduced stock was largely distributed in Rikaze of Tibet, Haixi of Qinghai Province, and Yushu of Sichuan Province. Under the economic growth scenario, new carbon stocks primarily occurred in Ali (Tibet), Haixi (Qinghai), and Kashgar (Xinjiang). In the environmental preservation scenario, the primary areas witnessing the emergence of new carbon stocks were Ali in Tibet, as well as Linzhi and Ganzi in Sichuan. Conversely, under the holistic progression scenario, the bulk of new carbon stocks were concentrated in Ali in Tibet and in Linzhi and Ganzi in Sichuan (Figure 6). In regard to land-use types, relative to the figures from 2020, carbon stocks in cultivated land and construction land exhibited increases across all scenarios. Carbon stocks in forest land declined solely under the economic growth scenario, while carbon stocks in grassland experienced growth exclusively under the economic growth scenario. Carbon stocks in water bodies remained largely stable across all scenarios (Table 10).

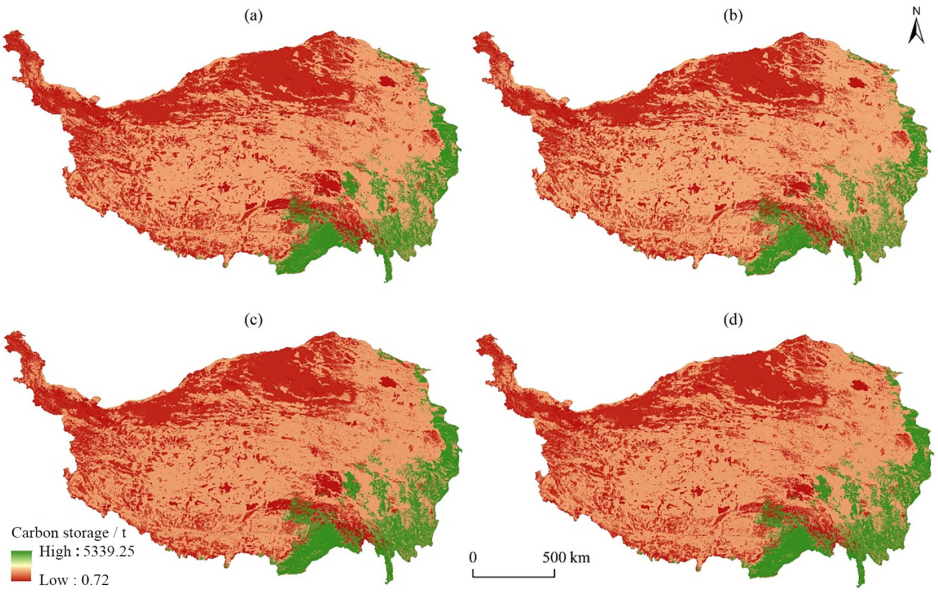

Figure 6. Carbon storage distribution in the Qinghai-Tibet Plateau under the different development scenarios in 2030. (**a**) Inherent progression scenario; (**b**) Economic growth scenario; (**c**) Environmental preservation scenario; (**d**) Holistic progression scenario.

Table 10. Carbon storage of the land-use types in the Qinghai-Tibet Plateau under the different development scenarios in 2030.

Land Type	Inherent Progression		Economic Growth		Environmental Preservation		Holistic Progression	
	Carbon Storage/10^8 t	Proportion/%	Carbon Storage/10^8 t	Proportion/%	Carbon Storage/10^8 t	Proportion/%	Carbon Storage/10^8 t	Proportion/%
Cultivated land	5.12	1.23	5.64	1.35	4.61	1.06	5.64	1.28
Forest land	151.38	36.49	136.29	32.58	166.52	38.24	166.52	37.87
Grassland	244.72	58.99	264.04	63.13	251.99	57.87	255.31	58.06
Water	0.01	0.00	0.01	0.00	0.02	0.00	0.01	0.00
Construction land	0.04	0.01	0.04	0.01	0.03	0.01	0.03	0.01
Unused land	13.61	3.28	12.25	2.93	12.25	2.81	12.25	2.79
Total	414.89	100.00	418.26	100.00	435.42	100.00	439.76	100.00

Concerning the carbon stocks of different carbon pool types, the integrated development scenario boasted the highest carbon stock, with the soil organic carbon pool totaling 19.435 billion tons. In contrast, the inherent progression scenario exhibited the lowest carbon stock, with the litterfall organic carbon pool amounting to 1.415 billion tons (Table 11). The belowground biomass organic carbon pool experienced its most substantial increase, reaching 5.59%, under the integrated development scenario. Conversely, the litterfall organic carbon pool recorded its most significant decrease, declining by 3.02%, under the inherent progression scenario.

Table 11. Carbon storage of the carbon pools in the Qinghai-Tibet Plateau under the different development scenarios in 2030.

Carbon Pool Type	Inherent Progression (10^8 t)	Economic Growth (10^8 t)	Environmental Preservation (10^8 t)	Holistic Progression (10^8 t)
Aboveground biomass organic carbon	59.90	59.52	63.61	64.10
Belowground biomass organic carbon	155.13	153.53	164.99	166.33
Litterfall organic carbon	14.15	14.63	14.78	14.98
Soil organic carbon	185.71	190.58	192.02	194.35

4.5. Spatial Autocorrelation Analysis of the Carbon Stocks in the Tibetan Plateau

Under the inherent progression, economic growth, environmental preservation, and holistic progression scenarios, Moran's I values of the carbon stocks in the Tibetan Plateau were 0.813, 0.807, 0.817, and 0.817, respectively, which indicates a high positive spatial correlation. Areas characterized by high values were primarily concentrated in regions with elevated temperature and precipitation levels, notably Sichuan, Yunnan, and southern Gansu. Conversely, regions with low values were concentrated in areas experiencing lower levels of precipitation and temperature, such as northern Tibet, southern Xinjiang, and northern Gansu (Figure 7).

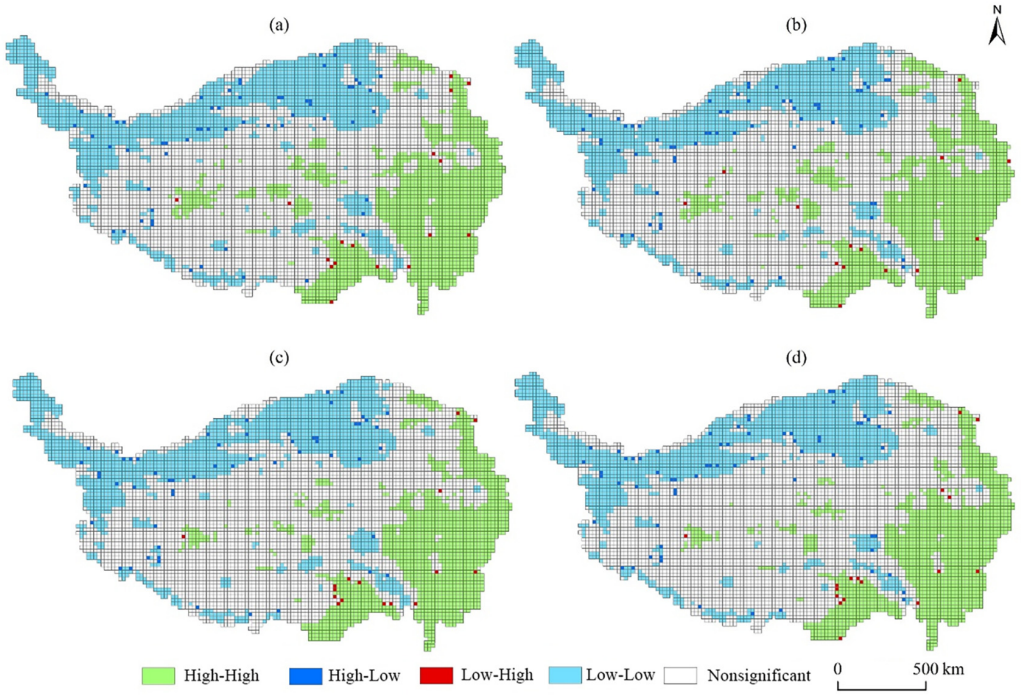

Figure 7. Local spatial autocorrelation of carbon storage in the Qinghai-Tibet Plateau under the different development scenarios. (**a**) Inherent progression scenario; (**b**) Economic growth scenario; (**c**) Environmental preservation scenario; (**d**) Holistic progression scenario.

5. Discussion

Land use has emerged as the predominant factor influencing the spatial distribution of carbon stocks, highlighting the importance of investigating land-use alterations in understanding the spatial and temporal dynamics of carbon stocks within terrestrial ecosystems [54]. For this study, we utilized the integration of the GMMOP and PLUS models to predict land-use changes in the Tibetan Plateau region up to the year 2030, spanning four distinct development scenarios. Additionally, the investigation assessed carbon stock dynamics from 2000 to 2020 and projected the spatial distribution of carbon stocks in 2030 under different scenarios, employing the InVEST model. Results indicated that between 2000 and 2020, there were increments in cultivated land, forest land, water, construction land, and unused land areas by 0.16%, 0.21%, 0.75%, 0.08%, and 2.38%, respectively. However, there was a decrease of 3.57% in the grassland area during the same period (Table 6). These results align with the conclusions drawn by Xu Runhong et al. (2023) regarding land-use changes in the Tibetan Plateau [55]. The carbon stock in the Tibetan Plateau exhibited a decline from 44.249 to 42.355 billion t. It is worth noting that this figure deviates slightly from the findings of Li Ruowei et al. (2021) regarding the carbon stock in the Tibetan Plateau [56]. The primary reason for this discrepancy is the difference in the definition of depth for biomass and soil organic carbon in the subsurface. In this study, the depth is defined as 0–100 cm, whereas Li Ruowei et al. (2021) may have defined it differently, possibly as 0–30 cm. As noted by Hao et al. (2023) [57], the carbon stock in the Qinghai-Tibet Plateau has shown a declining trend. Wang et al. (2019) reached the same conclusion through a review and synthesis of previous studies [58]. These findings are consistent with the results of our research. This variation in depth definition can lead to differences in the estimation of carbon stocks in the Tibetan Plateau. The spatial distribution analysis indicated a decreasing trend in the density of carbon stocks in the Tibetan Plateau from southeast to northwest. This observation aligns with the conclusions drawn by Shen et al. [59], further validating the consistency of findings across various studies. The mean values of the aboveground biomass, belowground biomass, litterfall, and soil organic carbon stocks in the Tibetan Plateau in 2030 under each scenario were 6.178 billion t, 16.00 billion t, 1.464 billion t, and 19.067 billion t, respectively, which occur between the values reported by Ding et al. (2019) [60] and Wang et al. (2023) [61]. In this study, carbon stocks were calculated using the InVEST model, whereas the resource inventory method was used in the above studies, with differences in the statistical approach. The findings of this study suggest a persistent decrease in the grassland area in the Tibetan Plateau until 2030 under the inherent progression scenario. However, this prediction diverges from the forecast made by Hao et al. (2023) [62]. Hao et al. determined that in the Yarlung Tsangpo River Basin of Tibet, the grassland area would exhibit an expanding trend up until 2038 in the inherent progression scenario. Conversely, both forest land and watershed areas would display contraction trends. In the environmental preservation scenario, the grassland area expanded while cultivated land decreased. This deviation stems from variations in the study area's scale and the diverse settings of land-use transformation rules. These differences lead to varying trends in land-use change.

The Tibetan Plateau region is predominantly covered by grassland, serving as a crucial component of the region's carbon sink [63]. It constitutes approximately 60.86% to 63.25% of the total carbon stock. The primary factor contributing to carbon loss is the conversion of grassland to land types with lower carbon storage capacities. Forest land, characterized by the highest carbon density per unit area, contributes 33.36% to 35.07% of the total carbon stock in the region. Despite a rise in carbon stock in forest land from 2000 to 2020, this increase failed to counterbalance the carbon loss resulting from the conversion of substantial grassland into unused land. In the inherent progression scenario, the conversion of high-carbon-density land categories, such as woodland and grassland, to low-carbon-density land categories, like unused land, resulted in a persistent decline in the carbon stock by 2030. In the economic growth scenario, the decline in carbon stocks was alleviated by transforming a considerable portion of unused land into cultivated land and construction

land. Conversely, in the scenario focused on environmental preservation, a significant portion of unused land was transformed into watersheds and forested areas, leading to a considerable rise in carbon stocks by the year 2030. Under the integrated development scenario, which emphasizes a blend of economic and ecological considerations, the forest land attained the highest integrated value coefficient. This scenario witnessed a significant conversion of unused land and grassland into forest land, thereby contributing to the highest carbon stock levels.

This research integrates the GMMOP, PLUS, and InVEST models to assess and predict carbon stocks in the Qinghai-Tibet Plateau. The combination of these models is relatively rare, and the effectiveness of this approach requires further validation and exploration. The research framework is broadly applicable and can be utilized in various fields such as land management planning, ecological planning, and ecosystem services. Compared with existing research frameworks, the superiority of this method lies in the following aspects: (1) The GMMOP model not only fully expresses the decision-makers' preferences but also has the advantage of being able to flexibly respond to policy changes and to make corresponding adjustments. Decision-makers can adjust model parameters based on the latest policy changes and external conditions to promptly obtain new optimal land-use allocation schemes. (2) By using the gray model to predict the future economic and ecological values of different land-use types, the method provides a theoretical reference for future land-use optimization. (3) By correcting carbon density, the precision of carbon stock evaluation is improved.

This research amalgamated ecological, economic, and social factors to enhance the quantitative structure and spatial arrangement of land utilization. Through the simulation of development scenarios via constraint settings, it predicted the distributions of land use and carbon stock in the study area. This approach fully leveraged the strengths of both models in structural optimization, scenario configuration, and spatial allocation, effectively circumventing the uncertainties and limitations associated with a singular model. Furthermore, the simulation results achieved a kappa coefficient of 0.80, indicating a high level of accuracy. These outcomes serve as a valuable reference for assessing carbon stocks in the Tibetan Plateau. Given the high geographic variability and ecological heterogeneity of the Qinghai-Tibet Plateau, this study combines the GMMOP and PLUS models to assess and predict its carbon stocks. In future research, more rigorous accuracy testing will be necessary to validate the results' effectiveness. The Qinghai-Tibet Plateau spans six provinces, each with different land-use policies, making it challenging to incorporate a unified land-use policy into the model for research. Future studies should aim to account for the impact of these varying land-use policies as much as possible. The basis for various climate change scenarios is the increase in carbon dioxide emissions caused by human activities. Changes in plant communities and, ultimately, land use will affect the carbon sequestration capacity of ecosystems [64]. This study has not yet considered climate change models. In future research, we will further incorporate climate change models to deeply explore the dynamics and trends of carbon stock changes in the Qinghai-Tibet Plateau.

6. Conclusions

The study evaluated the spatial and temporal distributions of carbon stocks in the Qinghai–Tibetan Plateau, utilizing land-use data spanning from 2000 to 2020. It employed coupled GMMOP and PLUS models to forecast land use and carbon stocks in the study area under various scenarios for the year 2030.

(1) Between 2000 and 2020, the Tibetan Plateau witnessed a decrease in grassland area, whereas cultivated land, forest land, water bodies, construction land, and unused land areas all expanded. Notably, under the inherent progression scenario, the grassland area experienced a considerable decline. Conversely, in the economic growth scenario, cultivated land, grassland, and construction land areas exhibited significant increases. In the environmental preservation scenario, there were notable increments in forest land and water areas, alongside reductions in grassland and unused land areas.

Finally, the holistic progression scenario saw substantial expansions in cultivated land, forest land, and construction land areas.

(2) Between 2000 and 2020, the total carbon stock decreased from 44.249 to 42.355 billion t. The grassland carbon stock decreased by 2.210 billion t, while the cultivated land, forest land, watershed, construction land, and unused land carbon stocks increased by 0.066 billion t, 0.92 billion t, 2.674 million t, 15.850 million t, and 156 million t, respectively. The average carbon stock of the soil organic carbon pool was the highest, recorded at 19.563 billion t, whereas the average carbon stock of the organic carbon pool of litterfall matter was the lowest, amounting to 1.507 billion t.

(3) In 2020, the total carbon stock witnessed a decrease of 866 Mt and 529 Mt under the inherent progression and economic growth scenarios, respectively. Conversely, it experienced an increase of 1187 Mt and 1621 Mt under the environmental preservation and integrated development scenarios, respectively. Notably, the soil organic carbon pool reached its peak under the integrated development scenario, totaling 19,435 Mt. In contrast, the litterfall organic carbon pool was at its lowest under the inherent progression scenario, registering at 1415 Mt. Additionally, the belowground biomass organic carbon pool exhibited the most significant growth under the integrated development scenario, with an increase of 5.59%.

Author Contributions: Conceptualization, J.X. and L.Y.; methodology, L.Y.; software, B.F.; validation, B.F.; formal analysis, B.F.; investigation, B.F.; resources, L.Y.; data curation, B.F.; writing—original draft preparation, J.X. and B.F.; writing—review and editing, J.X.; visualization, B.F.; supervision, L.Y.; project administration, L.Y.; funding acquisition, J.X. All authors have read and agreed to the published version of the manuscript.

Funding: This research was funded by the National Social Science Fund of China (23BJY198).

Institutional Review Board Statement: Not applicable.

Informed Consent Statement: Not applicable.

Data Availability Statement: The original contributions presented in the study are included in the article; further inquiries can be directed to the corresponding author.

Conflicts of Interest: The authors declare no conflicts of interest.

References

1. Lal, R.; Smith, P.; Jungkunst, H.F.; Mitsch, W.J.; Lehmann, J.; Nair, P.R.; McBratney, A.B.; de Moraes Sá, J.C.; Schneider, J.; Zinn, Y.L. The carbon sequestration potential of terrestrial ecosystems. *J. Soil Water Conserv.* **2018**, *73*, 145A–152A. [CrossRef]
2. Sun, B.; Du, J.; Chong, F.; Li, L.; Zhu, X.; Zhai, G.; Song, Z.; Mao, J. Spatio-temporal variation and prediction of carbon storage in terrestrial ecosystems in the yellow river basin. *Remote Sens.* **2023**, *15*, 3866. [CrossRef]
3. Zafar, Z.; Zubair, M.; Zha, Y.; Mehmood, M.S.; Rehman, A.; Fahd, S.; Nadeem, A.A. Predictive modeling of regional carbon storage dynamics in response to land use/land cover changes: An InVEST-based analysis. *Ecol. Inform.* **2024**, *82*, 102701. [CrossRef]
4. Zhu, L.; Song, R.; Sun, S.; Li, Y.; Hu, K. Land use/land cover change and its impact on ecosystem carbon storage in coastal areas of China from 1980 to 2050. *Ecol. Indic.* **2022**, *142*, 109178. [CrossRef]
5. Heimann, M.; Reichstein, M. Terrestrial ecosystem carbon dynamics and climate feedbacks. *Nature* **2008**, *451*, 289–292. [CrossRef]
6. Li, Y.; Liu, Z.; Li, S.; Li, X. Multi-scenario simulation analysis of land use and carbon storage changes in changchun city based on FLUS and InVEST model. *Land* **2022**, *11*, 647. [CrossRef]
7. Fang, J.; Chen, A.; Peng, C.; Zhao, S.; Ci, L. Changes in forest biomass carbon storage in China between 1949 and 1998. *Science* **2001**, *292*, 2320–2322. [CrossRef] [PubMed]
8. Fang, J.Y.; Wang, G.G.; Liu, G.H.; Xu, S.L. Forest biomass of China: An estimate based on the biomass–volume relationship. *Ecol. Appl.* **1998**, *8*, 1084–1091.
9. Wu, Q.; Wu, F.; Tan, B.; Yang, W.; Ni, X.; Yang, Y. Carbon, nitrogen and phosphorus stocks in soil organic layer as affected by forest gaps in the alpine forest of the eastern Tibet Plateau. *Russ. J. Ecol.* **2015**, *46*, 246–251. [CrossRef]
10. Zhang, Y.; Zhao, Y.; Shi, X.; Lu, X.; Yu, D.; Wang, H.; Sun, W.; Darilek, J. Variation of soil organic carbon estimates in mountain regions: A case study from Southwest China. *Geoderma* **2008**, *146*, 449–456. [CrossRef]
11. Williams, D.R.; Alvarado, F.; Green, R.E.; Manica, A.; Phalan, B.; Balmford, A. Land-use strategies to balance livestock production, biodiversity conservation and carbon storage in Yucatán, Mexico. *Glob. Chang. Biol.* **2017**, *23*, 5260–5272. [CrossRef] [PubMed]

12. Searchinger, T.D.; Wirsenius, S.; Beringer, T.; Dumas, P. Assessing the efficiency of changes in land use for mitigating climate change. *Nature* **2018**, *564*, 249–253. [CrossRef] [PubMed]
13. Zhang, Z.; Hörmann, G.; Huang, J.; Fohrer, N. A random forest-based CA-Markov model to examine the dynamics of land use/cover change aided with remote sensing and GIS. *Remote Sens.* **2023**, *15*, 2128. [CrossRef]
14. Liu, D.; Zheng, X.; Wang, H. Land-use simulation and decision-support system (LandSDS): Seamlessly integrating system dynamics, agent-based model, and cellular automata. *Ecol. Modell.* **2020**, *417*, 108924. [CrossRef]
15. Bütikofer, L.; Adde, A.; Urbach, D.; Tobias, S.; Huss, M.; Guisan, A.; Randin, C. High-resolution land use/cover forecasts for Switzerland in the 21st century. *Sci. Data* **2024**, *11*, 231. [CrossRef]
16. Lin, W.; Sun, Y.; Nijhuis, S.; Wang, Z. Scenario-based flood risk assessment for urbanizing deltas using future land-use simulation (FLUS): Guangzhou Metropolitan Area as a case study. *Sci. Total Environ.* **2020**, *739*, 139899. [CrossRef]
17. Zhang, S.; Yang, P.; Xia, J.; Wang, W.; Cai, W.; Chen, N.; Hu, S.; Luo, X.; Li, J.; Zhan, C. Land use/land cover prediction and analysis of the middle reaches of the Yangtze River under different scenarios. *Sci. Total Environ.* **2022**, *833*, 155238. [CrossRef]
18. Liang, X.; Guan, Q.; Clarke, K.C.; Liu, S.; Wang, B.; Yao, Y. Understanding the drivers of sustainable land expansion using a patch-generating land use simulation (PLUS) model: A case study in Wuhan, China. *Comput. Environ. Urban Syst.* **2021**, *85*, 101569. [CrossRef]
19. Lai, Z.; Chen, C.; Chen, J.; Wu, Z.; Wang, F.; Li, S. Multi-scenario simulation of land-use change and delineation of urban growth boundaries in county area: A case study of Xinxing County, Guangdong Province. *Land* **2022**, *11*, 1598. [CrossRef]
20. Li, Q.; Gao, M.; Li, J. Carbon emissions inventory of farm size pig husbandry combining Manure-DNDC model and IPCC coefficient methodology. *J. Cleaner Prod.* **2021**, *320*, 128854.
21. Bagstad, K.; Villa, F.; Johnson, G.; Voigt, B. *ARIES–Artificial Intelligence for Ecosystem Services: A Guide to Models and Data, Version 1.0*; ARIES report series 1; 2011. Available online: https://www.bioecon-network.org/pages/11th_2009/Villa.pdf (accessed on 3 July 2024).
22. Duan, H.; Xu, N. Assessing social values for ecosystem services in rural areas based on the SolVES model: A case study from Nanjing, China. *Forests* **2022**, *13*, 1877. [CrossRef]
23. Gao, F.; Xin, X.; Song, J.; Li, X.; Zhang, L.; Zhang, Y.; Liu, J. Simulation of LUCC dynamics and estimation of carbon stock under different SSP-RCP scenarios in Heilongjiang Province. *Land* **2023**, *12*, 1665. [CrossRef]
24. Jia, X.; Zhu, J.; Li, Y.; Wu, W.; Hu, X. Analysis of the driving role and impact of road construction on carbon stock. *Environ. Sci. Pollut. Res.* **2023**, *30*, 67131–67149. [CrossRef]
25. Nyamari, N.; Cabral, P. Impact of land cover changes on carbon stock trends in Kenya for spatial implementation of REDD+ policy. *Appl. Geog.* **2021**, *133*, 102479. [CrossRef]
26. Cao, L.; Huo, X.; Xiang, J.; Lu, L.; Liu, X.; Song, X.; Jia, C.; Liu, Q. Interactions and marginal effects of meteorological factors on haemorrhagic fever with renal syndrome in different climate zones: Evidence from 254 cities of China. *Sci. Total Environ.* **2020**, *721*, 137564. [CrossRef]
27. Liu, Y.; Yu, G.; Wang, Q.; Zhang, Y. How temperature, precipitation and stand age control the biomass carbon density of global mature forests. *Glob. Ecol. Biogeogr.* **2014**, *23*, 323–333. [CrossRef]
28. Wei, Y.; Yi, M.; Yu, Y.; You, Y.; Zhang, W.; Li, R.; Yu, C.; Wang, S. Global drivers of timber carbon stock from income-based perspective. *Front. Environ. Sci.* **2023**, *11*, 1149492. [CrossRef]
29. Hu, B.; Zhang, P.; Bai, N.; Zhao, L. Land use scenario simulation in Qinglong Manchu Autonomous County based on CLUE-S and GMOP model. *Chin. J. Agric. Resour. Reg. Plan* **2020**, *41*, 173–182.
30. Bacani, V.M.; da Silva, B.H.M.; Sato, A.A.d.S.A.; Sampaio, B.D.S.; da Cunha, E.R.; Vick, E.P.; de Oliveira, V.F.R.; Decco, H.F. Carbon storage and sequestration in a eucalyptus productive zone in the Brazilian Cerrado, using the Ca-Markov/Random Forest and InVEST models. *J. Clean. Prod.* **2024**, *444*, 141291. [CrossRef]
31. Xie, L.; Bai, Z.; Yang, B.; Fu, S. Simulation analysis of land-use pattern evolution and valuation of terrestrial ecosystem carbon storage of Changzhi City, China. *Land* **2022**, *11*, 1270. [CrossRef]
32. Li, C.; Wu, Y.; Gao, B.; Zheng, K.; Wu, Y.; Li, C. Multi-scenario simulation of ecosystem service value for optimization of land use in the Sichuan-Yunnan ecological barrier, China. *Ecol. Indic.* **2021**, *132*, 108328. [CrossRef]
33. Du, Y.; Li, X.; He, X.; Li, X.; Yang, G.; Li, D.; Xu, W.; Qiao, X.; Li, C.; Sui, L. Multi-scenario simulation and trade-off analysis of ecological service value in the Manas River Basin based on land use optimization in China. *Int. J. Environ. Res. Public Health* **2022**, *19*, 6216. [CrossRef] [PubMed]
34. Wang, Y.; Lü, Y.; Lü, D.; Wang, C.; Wu, X.; Yin, L.; Wang, X. Carbon and water relationships change nonlinearly along elevation gradient in the Qinghai Tibet Plateau. *J. Hydrol.* **2024**, *628*, 130529. [CrossRef]
35. Li, X.; Wu, T.; Zhu, X.; Jiang, Y.; Hu, G.; Hao, J.; Ni, J.; Li, R.; Qiao, Y.; Yang, C. Improving the Noah-MP model for simulating hydrothermal regime of the active layer in the permafrost regions of the Qinghai-Tibet Plateau. *J. Geophys. Res. Atmos.* **2020**, *125*, e2020JD032588. [CrossRef]
36. Piao, S.; Zhang, X.; Wang, T.; Liang, E.; Wang, S.; Zhu, J.; Niu, B. Responses and feedback of the Tibetan Plateau's alpine ecosystem to climate change. *Chin. Sci. Bull.* **2019**, *64*, 2842–2855. [CrossRef]

37. Liu, G.; Zhao, L.; Xie, C.; Zou, D.; Wu, T.; Du, E.; Wang, L.; Sheng, Y.; Zhao, Y.; Xiao, Y. The zonation of mountain frozen ground under aspect adjustment revealed by ground-penetrating radar survey—A case study of a small catchment in the upper reaches of the Yellow River, Northeastern Qinghai-Tibet Plateau. *Remote Sens.* **2022**, *14*, 2450. [CrossRef]
38. Zhao, L.; Hu, G.; Liu, G.; Zou, D.; Wang, Y.; Xiao, Y.; Du, E.; Wang, C.; Xing, Z.; Sun, Z. Investigation, monitoring, and simulation of permafrost on the Qinghai-Tibet Plateau: A review. *Permafr. Periglac. Process.* **2024**. Available online: https://onlinelibrary.wiley.com/doi/abs/10.1002/ppp.2227 (accessed on 3 July 2024). [CrossRef]
39. Ma, Y.J.; Li, X.Y.; Liu, L.; Huang, Y.M.; Li, Z.; Hu, X.; Wu, X.C.; Yang, X.F.; Wang, P.; Zhao, S.J. Measurements and modeling of the water budget in semiarid high-altitude Qinghai Lake Basin, Northeast Qinghai-Tibet plateau. *J. Geophys. Res. Atmos.* **2018**, *123*, 10,857–10,871. [CrossRef]
40. Li, D.S.; Cui, B.L.; Wang, Y.; Wang, Y.X.; Jiang, B.F. Source and quality of groundwater surrounding the Qinghai Lake, NE Qinghai-Tibet Plateau. *Groundwater* **2021**, *59*, 245–255. [CrossRef]
41. Alam, S.A.; Starr, M.; Clark, B.J. Tree biomass and soil organic carbon densities across the Sudanese woodland savannah: A regional carbon sequestration study. *J. Arid. Environ.* **2013**, *89*, 67–76. [CrossRef]
42. Yang, J.; Xie, B.P.; Zhang, D.G. Spatio-temporal evolution of carbon stocks in the Yellow River Basin based on InVEST and CA-Markov models. *Chin. J. Eco-Agric.* **2021**, *29*, 1018–1029.
43. Li, K.; Cao, J.; Adamowski, J.F.; Biswas, A.; Zhou, J.; Liu, Y.; Zhang, Y.; Liu, C.; Dong, X.; Qin, Y. Assessing the effects of ecological engineering on spatiotemporal dynamics of carbon storage from 2000 to 2016 in the Loess Plateau area using the InVEST model: A case study in Huining County, China. *Environ. Dev.* **2021**, *39*, 100641. [CrossRef]
44. Wang, Y.; Li, X.; Zhang, Q.; Li, J.; Zhou, X. Projections of future land use changes: Multiple scenarios-based impacts analysis on ecosystem services for Wuhan city, China. *Ecol. Indic.* **2018**, *94*, 430–445. [CrossRef]
45. Cao, S.; Jin, X.B.; Yang, X.H.; Sun, R.; Liu, J.; Han, B.; Xu, W.Y.; Zhou, Y.K. Coupled MOP and GeoSOS-FLUS models research on optimization of land use structure and layout in Jintan district. *J. Nat. Resour.* **2019**, *34*, 1171–1185. [CrossRef]
46. Xie, G.D.; Zhang, C.X.; Zhang, L.M.; Chen, W.H.; Li, S.M. Improvement of the evaluation method for ecosystem service value based on per unit area. *J. Nat. Resour.* **2015**, *30*, 1243–1254.
47. Zheng, W.; Ke, X.; Xiao, B.; Zhou, T. Optimising land use allocation to balance ecosystem services and economic benefits-A case study in Wuhan, China. *J. Environ. Manag.* **2019**, *248*, 109306. [CrossRef]
48. Yanfang, L.; Dongping, M.; Jianyu, Y. Optimization of land use structure based on ecological GREEN equivalent. *Geo-Spat. Inf. Sci.* **2002**, *5*, 60–67. [CrossRef]
49. Pal, S.; Bauch, C.T.; Anand, M. Coupled social and land use dynamics affect dietary choice and agricultural land-use extent. *Commun. Earth Environ.* **2021**, *2*, 204. [CrossRef]
50. Qu, Y.; Long, H. The economic and environmental effects of land use transitions under rapid urbanization and the implications for land use management. *Habitat Int.* **2018**, *82*, 113–121. [CrossRef]
51. Liu, X.; Liang, X.; Li, X.; Xu, X.; Ou, J.; Chen, Y.; Li, S.; Wang, S.; Pei, F. A future land use simulation model (FLUS) for simulating multiple land use scenarios by coupling human and natural effects. *Landsc. Urban Plan.* **2017**, *168*, 94–116. [CrossRef]
52. Xu, L.; Liu, X.; Tong, D.; Liu, Z.; Yin, L.; Zheng, W. Forecasting urban land use change based on cellular automata and the PLUS model. *Land* **2022**, *11*, 652. [CrossRef]
53. Meimei, W.; Zizhen, J.; Tengbiao, L.; Yongchun, Y.; Zhuo, J. Analysis on absolute conflict and relative conflict of land use in Xining metropolitan area under different scenarios in 2030 by PLUS and PFCI. *Cities* **2023**, *137*, 104314. [CrossRef]
54. Wang, H.; Jin, H.; Li, X.; Zhou, L.; Qi, Y.; Huang, C.; He, R.; Zhang, J.; Yang, R.; Luo, D. Changes in carbon stock in the Xing'an permafrost regions in Northeast China from the late 1980s to 2020. *GISci. Remote Sens.* **2023**, *60*, 2217578. [CrossRef]
55. Xu, R.; Shi, P.; Gao, M.; Wang, Y.; Wang, G.; Su, B.; Huang, J.; Lin, Q.; Jiang, T. Projected land use changes in the Qinghai-Tibet Plateau at the carbon peak and carbon neutrality targets. *Sci. China Earth Sci.* **2023**, *66*, 1383–1398. [CrossRef]
56. Li, R.W.; Ye, C.C.; Wang, Y.; Han, G.D.; Sun, J. Carbon storage estimation and its drivering force analysis based on InVEST model in the Tibetan Plateau. *Acta Agrestia Sin.* **2021**, *29*, 43.
57. Hao, J.Y.; Zhi, L.; Li, X.; Dong, S.K.; Li, W. Temporal and spatial variations and the relationships of land use pattern and ecosystem services in Qinghai-Tibet Plateau, China. *J. Appl. Ecol.* **2023**, *34*, 3053–3063.
58. Wang, L.; Zeng, H.; Zhang, Y.J.; Zhao, G.; Chen, N.; Li, J.X. A review of research on soil carbon storage and its influencing factors in the Tibetan Plateau. *Chin. J. Ecol.* **2019**, *38*, 3506.
59. Shen, X.; Liu, Y.; Zhang, J.; Wang, Y.; Ma, R.; Liu, B.; Lu, X.; Jiang, M. Asymmetric impacts of diurnal warming on vegetation carbon sequestration of marshes in the Qinghai Tibet Plateau. *Glob. Biogeochem. Cycles* **2022**, *36*, e2022GB007396. [CrossRef]
60. Ding, J.; Wang, T.; Piao, S.; Smith, P.; Zhang, G.; Yan, Z.; Ren, S.; Liu, D.; Wang, S.; Chen, S. The paleoclimatic footprint in the soil carbon stock of the Tibetan permafrost region. *Nat. Commun.* **2019**, *10*, 4195. [CrossRef]
61. Wang, T.; Wang, X.; Liu, D.; Lv, G.; Ren, S.; Ding, J.; Chen, B.; Qu, J.; Wang, Y.; Piao, S.; et al. The current and future of terrestrial carbon balance over the Tibetan Plateau. *Sci. China Earth Sci.* **2023**, *66*, 1493–1503. [CrossRef]
62. Hao, W.; Cao, Z.; Ou, S.; Qin, Y.; Wang, Z.; Yang, S.; Tiando, D.S.; Fan, X. A simulation analysis of land use changes in the Yarlung Zangbo River and its two tributaries of Tibet using the Markov–PLUS model. *Sustainability* **2023**, *15*, 1376. [CrossRef]

63. Fayiah, M.; Dong, S.; Khomera, S.W.; Ur Rehman, S.A.; Yang, M.; Xiao, J. Status and challenges of Qinghai-Tibet Plateau's grasslands: An analysis of causes, mitigation measures, and way forward. *Sustainability* **2020**, *12*, 1099. [CrossRef]
64. Wang, K.; Li, X.; Lyu, X.; Dang, D.; Dou, H.; Li, M.; Liu, S.; Cao, W. Optimizing the land use and land cover pattern to increase its contribution to carbon neutrality. *Remote Sens.* **2022**, *14*, 4751. [CrossRef]